

Coating of Nano-film Cr_2O_3 on Welded 304L Stainless Steel and Its Surface Resistance Properties

Nattapong Dussadeeworrarak¹, Pocharapon Silakoo², Attaphon Kaewvilai¹ and Thammanoon Thawechai^{3*}

¹ Department of Welding Engineering Technology, College of Industrial Technology, King Mongkut's University of Technology North Bangkok

² Thai-German Pre-Engineering School, College of Industrial Technology, King Mongkut's University of Technology North Bangkok

³ School of Integrated Science, Kasetsart University

* Corresponding author, E-mail: sistnt@ku.ac.th

Received: 5 October 2021; Revised 18 November 2021; Accepted: 19 November 2021

Online Published: 24 November 2021

Abstract: This research presented the Cr_2O_3 coating and surface properties of welded stainless steel pipe grade 304L. For the welding, process, the 304L specimen was prepared with a single V-butt joint and welded by the tungsten inert gas (TIG) welding process. The weld quality was investigated by visual test (VT), penetrant test (PT) and radiographic test (RT), respectively. After that, the welded specimen was coated with colored-oxide film by chromic reduction. The structural phase and crystallite size of the coated film on welded 304L (C-304L) were analyzed by X-ray diffractometer (XRD) and calculated by Scherrer's equation. The atomic force microscope (AFM) was used for measuring the thickness of the Cr_2O_3 film. In addition, the surface properties such as hardness and electrical resistance of the coated specimens were tested by Vickers hardness tester and digital multi-meter. Finally, the corrosion resistance of specimens before and after surface coating was determined in extremely corrosive condition such as chlorinated sulfuric acid. The results showed that the C-304L has excellent surface resistance properties for erosion-corrosion applications.

Keywords: Nano-film Cr_2O_3 , Welded stainless steel; Oxidation; Surface resistance



1. Introduction

Stainless steel pipe-based ASME SA312 TP304L (304L) is austenitic steel consisting of chromium (Cr), nickel (Ni) and low carbon (C) contents with many excellent abilities such as mechanical properties, lightweight, and thermal-corrosion resistances [1-4]. It has been widely used in piping industrial applications such as chemical tanks, steam pipe for power generation, fluid transportation, etc [4-6]. It is easy for welding and fabrication by various welding processes such as friction stir welding (FSW), plasma arc welding (PAW), etc [5-10]. Among the various welding processes, gas tungsten arc welding (GTAW) also known as tungsten inert gas (TIG), is an efficient welding process for 304L which results in welding with high-quality and high penetration [5-8]. However, the welded stainless steel has been affected by welding heat and surface finishing which destroyed the passive film (stable film of chromium oxide) and decreased corrosion resistance property [11-13]. Especially, when those exposed to chloride ions and acid cause corrosion with uniform and pitting formations [6, 14-16]. Therefore, the surface properties of the welded 304L need to be improved before being used in applications under corrosive-erosive conditions.

Chromic oxidation is a kind of method for producing chromium oxide film coated on the

surface of stainless steel [16-18]. The chromium oxide film in different thicknesses can be grown on the surface of stainless steel and affect the stainless steel resulting in several film colors [16-18]. In addition, the coated film can also protect the stainless steel substrate from environmental damages [19-22]. Based on its color form and resistance properties, the surface coating of stainless steel by chromic oxidation has also been interested in a wide range of applications [16-22].

In this work, we have an idea of the coating of chromium oxide on welded 304L pipe (C-304L) by chemical reduction process of Cr^{+6} to Cr^{+3} as a Cr_2O_3 film to improve surface resistant properties. The coated film on the C-304L surface was analyzed by X-ray diffractometer (XRD) and atomic force microscope (AFM). In addition, the surface properties such as hardness, electrical resistance and corrosion resistance of the C-304L were investigated for considering the possibility of using C-304L in erosion-corrosion resistant applications.

2. Experimental Process

2.1 Materials

Stainless steel pipe (ASME SA312, TP304L) with thickness 2.8 mm were supported by KMUTNB. The thoriated tungsten electrode (EWTh-2, the diameter of 2.4 mm) and filler rod (AWS class ER308, the diameter of 2.4 mm)



were purchased from WELDMAX. Argon 99% product from Pacs Machanic System Co., LTD. was used as shielding and backing gasses for the tungsten inert gas welding process (TIG). The chemical agents purchased from Nabakem Mega Check were used for penetrant inspection. ASTM Type I water (ASTM D1193-06) [23] was used for all experiments. All chemicals such as sulfuric acid (H_2SO_4) dichromic acid ($H_2Cr_2O_7$), zinc sulfate ($ZnSO_4$), manganese sulfate mono hydrate ($MnSO_4 \cdot H_2O$), Sodium hydroxide (NaOH), Sodium Chloride (NaCl), acetone (C_3H_6O) and ammonium molybdate tetrahydrate ($(NH_4)_6Mo_7O_{24} \cdot 4H_2O$) were analytical grade from CARLO ERBA Reagents.

2.2 Instruments

TIG welding machine was obtained from LONGWELL as TIG215S model. Actual current, voltage and welding temperature were measured by multi-meter (UNI-T, UT200) and infrared thermo-sensor (PROSKIT, MT-4612). The visual test (VT; Weld gauge, Metric) and radiographic test (RT; X-ray radiographic tester, General Electric Corporation) were inspected as standard methods.

Table 1 Welding parameter for 304L

Welds	Polarity	Current	Voltage	Speed	Interpass Temp.	Heat Input	Gas Flow Rate
Root	DCEN	110 A	11 V	45 mm/min	30°C	1.7 kJ/mm	15 L/min
Hot	DCEN	120 A	12 V	90 mm/min	65°C	0.9 kJ/mm	15 L/min
Cover	DCEN	130 A	13 V	70 mm/min	85°C	1.5 kJ/mm	15 L/min

For the chemical reduction process and corrosion testing, the autolab series, PGSTAT302N model, was used as a potentiostat instrument. The phase component of the 304L after chromic reduction process welded 304L pipe (C-304L) was characterized by X-ray diffraction (XRD; a Philips X-Pert-MPD X-ray diffractometer) using $Cu-K\alpha$ ($\lambda = 1.5406 \text{ \AA}$) at the 2-theta of 30° to 80° with a scanning rate of 0.2 s^{-1} . The microstructure of the oxidized S304 was characterized by an atomic force microscope (AFM: ARMFP-3D). The hardness properties of the prepared specimens were measured by the Vickers microhardness tester (Wolpert Wilson Instruments).

2.3 Welding and Inspection

The joint of the 304L specimen was prepared as a single V-butt joint with a groove angle of 60° . The distances of root face and root opening were controlled at 2.0 mm 3.0 mm, respectively. The 304L was welded by the TIG welding process with the weaving technique, at a flat position. The numbers of weld passes (root, hot and cover), as well as the welding parameters with heating inputs, are summarized in Table 1.



The welded specimen was observed for the weld quality at the surface by VT and PT inspections. After that, the inside weld was inspected by RT with the double-wall technique using phosphate film (D7 class) and the exposure parameters of 140 kV, 6 mA, 30 seconds at the focus to film distance (FFD) of 700 mm. The RT image was developed by a computed scan.

2.4 Coating, Characterization, and Testing

The welded 304L was cut in the size of 20 x 50 mm for 4 specimens and polished by sandpaper at 1200 grit. The polished specimen was clean by acetone and dried at 60°C. The original passive film on S304L was eliminated by the immerse specimen in hot base solution (3N NaOH at 60°C) for 30 min, then cleaned by acetone and dried at 60°C. For surface oxidation, an oxidizing aqueous solution was prepared from the mixing of H₂SO₄ (490 g/L) and H₂Cr₂O₇ (250 g/L). The ZnSO₄ (5.0 g/L) and MnSO₄·H₂O (4.0 g/L) were dissolved in the mixed solution for accelerating and stabilizing the oxide film [17]. An (NH₄)₆Mo₇O₂₄·4H₂O (7.0 g/L) was further added into the solution for enhancing the adherence [17, 18] of oxide film on welded 304L surface. After that, the pretreated specimen was immersed in an oxidizing solution. Each specimen was prepared at different times of 4, 8 and 12 min. The obtained specimen was cleaned with de-ionized water and acetone.

The surface oxidized film on the welded specimen was analyzed by XRD to determine the phase structure and lattice parameters [24]. The crystallite size of the oxide structure was calculated by Scherrer's equation as followed: $D = \kappa \lambda / \beta \cos \theta$ where D is the crystallite size; K is a dimensionless shape factor (0.89); λ is the X-ray wavelength of Cu-K α radiation source (1.5406 Å); β is the full width at half maximum of diffraction peak in radians obtained from the peak fitting by Pearson 7 function in Fityk, a data processing software. This quantity is also denoted as $\Delta(2\theta)$ where θ is the Bragg angle [25, 26]. The morphologies of the C-304L at different oxidation times were also analyzed by AFM.

Furthermore, the correlation of film thickness with hardness and electrical properties of C-304L was analyzed. The corrosion of C-304L was tested in mixed solutions of 2M of H₂SO₄ and 5% NaCl [16] by using a potentiostat instrument according to ASTM: G5-14 standard method [27]. The probes of the working electrode (WE) and the counter electrode (CE) were graphite rods while the reference electrode (RE) was Ag/AgCl. The testing temperature was controlled at 25±1 °C. After completing the testing process, Tafel's plot was applied for analyzing the corrosion rate from the polarization curve.

3. Results and Discussion

3.1 Welding and Inspection

From visual and penetrant inspections, the welded pipe from TIG exhibited a good weld without defect and discontinued at the surface as shown in Fig. 1 (a) and (b). The weld dimension of the welded pipe was found approximately 10.0 mm width and 4.0 mm convex which was in the range according to ASME section VIII Div.1 [28]. From the radiographic test, the X-ray images of the welded specimen showed the two contrast zones, dark and brighten grey, which was assigned as the areas of base and weld, respectively (Fig. 1 (c)).

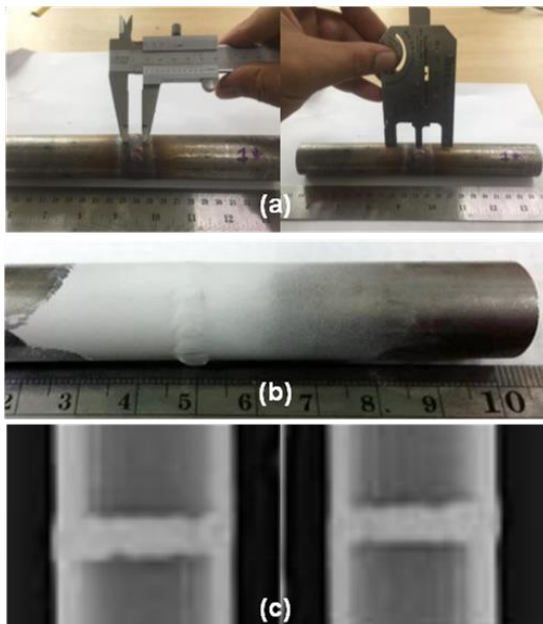


Fig. 1 Inspections of welded 304L:

(a) VT, (b) PT and (c) RT

The RT image of the welded specimen showed the completed weld and penetration without any defect observed at all of the areas. Form inspection testing results (VT, PT, and RT), indicated that the parameters of TIG (Table 1) could control the quality of 304L weld.

3.2 Oxidation, Characterization, and Testing

All surfaces (base and weld zones) of the obtained specimens after oxidation (C-304L) appeared as yellow, brown and blue colors for reaction times of 4, 8 and 12 min, (Fig. 2). It indicated that the oxide was coated on the welded 304L as coated oxide product (C-304L). In addition, it was found that the color of the specimen had not changed after oxidation over 12 min which might indicate that the thickness of oxide film on the specimen eventually reached a steady-state [16-18].

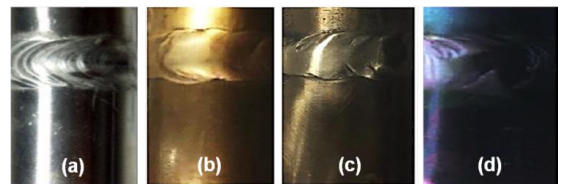


Fig. 2 The welded 304L (a) before and after oxidation at (b) 4, (c) 8 and (d) 12 min

By XRD characterization, the XRD patterns of C-304L (Fig. 3) showed the main peaks of austenitic stainless steel at 2θ of 44.69° , 50.97° and 75.87° according to the crystal structure of



face centered cubic (FCC) [18]. Moreover, the XRD spectrum of the C-304L also exhibited both peaks at 2θ of 36.53° and 46.91° which were implied to the peaks of chromium oxide in form Cr_2O_3 corresponded to the rhombohedral structure with JCPDS No. 72-3533 [24]. The lattice parameters were calculated and found $a, b = 4.69 \text{ \AA}$ and $c = 13.50 \text{ \AA}$ which was related to the kinds of literature [24, 29]. The crystallite size of Cr_2O_3 was analyzed at 2θ of 36.53° and 46.91° by Scherrer's equation and found to be 4.82 and 29.70 nm, respectively. According to the changing color on specimens and XRD results, it clearly confirmed that the surface of welded 304L was oxidation into the form of nano- Cr_2O_3 .

The morphological surface (average of thickness and roughness) of the C-304L at different times of chromic reduction was analyzed by AFM analysis as shown in Fig. 4. The results from AFM exhibited that all the specimens of C-304L consisted of surface roughness around $0.10 \pm 0.01 \mu\text{m}$. This implied that the increased time of oxidation had no effects on the surface morphologies of the C-304L, or in another word, it could be suggested that the oxide films of different oxidation times should exist in the same structural phases. However, the oxidation time influenced the thickness of the Cr_2O_3 film on the C-304L specimen significantly.

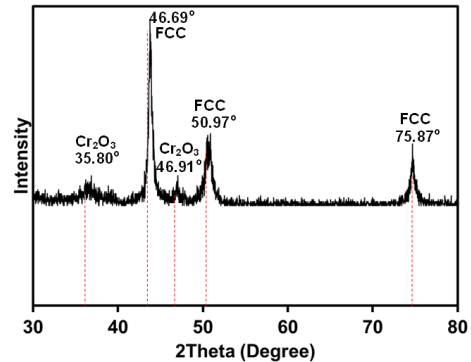


Fig. 3 XRD of welded 304L (a) before and (b) after oxidation at 12 min

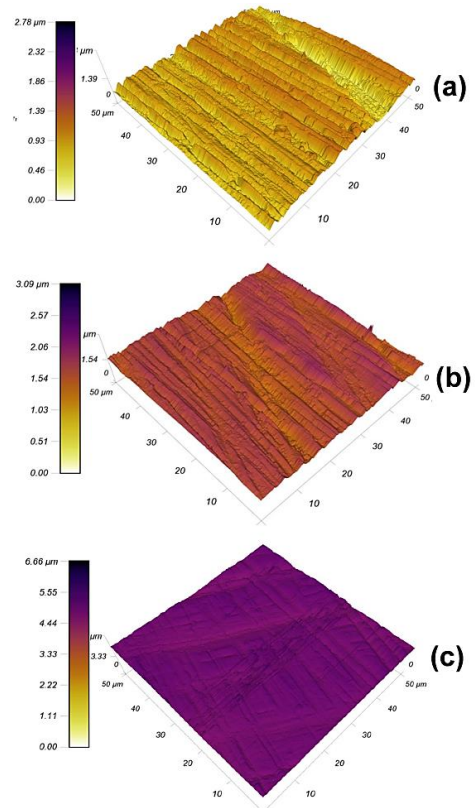


Fig. 4 AFM of welded 304L after oxidation at (a) 4, (b) 8 and (c) 12 min

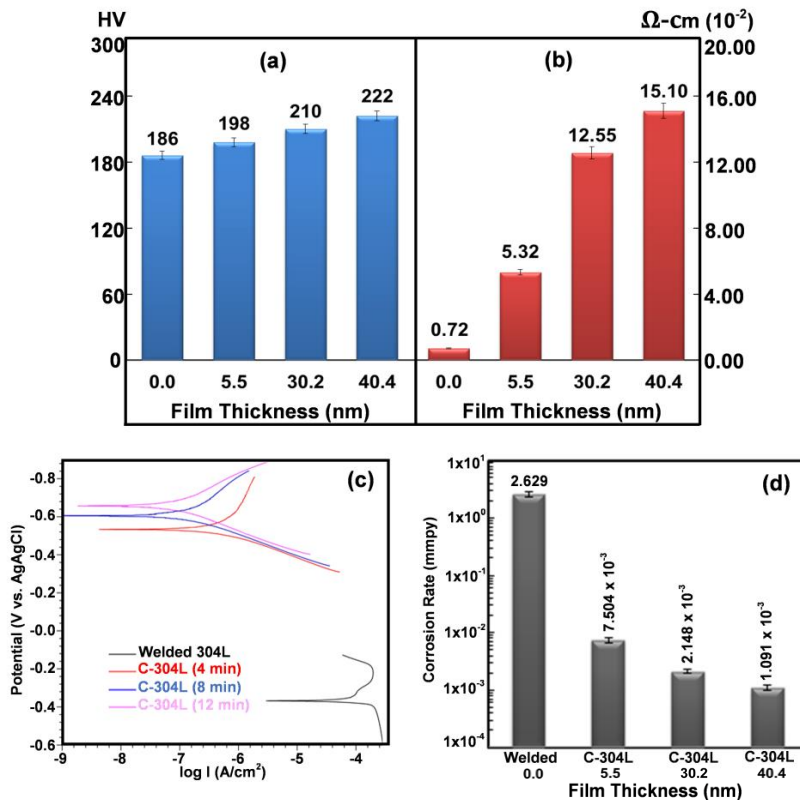


Fig. 5. The testing results of welded 304L and C-304L with various film thicknesses: (a) Hardness, (b) electrical resistivity, (c) polarization curves and (d) corrosion rate

The thickness of the Cr_2O_3 film increased with the increase of reaction time. The results exhibited that the film from the chromic reduction time of 4, 8 and 12 min consisted of the thickness around 5.5, 30.2 and 40.4 nm, respectively.

Fig. 5 (a) and (b) showed the results of hardness and electrical resistivity of 304L and C-304L with different thicknesses of oxide film. The hardness of 304L and C-304L with thickness film of 3.5, 29.0 and 40.3 nm was measured as

186, 198, 210 and 222 HV, respectively indicating that the hardness values of 304L surface were enhanced by the Cr_2O_3 film from the reduction of Cr^{+6} to Cr^{+3} . The electrical resistivity of 304L and C-304L with thickness film of 5.5, 30.2 and 40.4 nm was measured as 0.72×10^{-2} , 5.32×10^{-2} , 12.55×10^{-2} and $15.10 \times 10^{-2} \Omega\text{.cm}$, respectively. The result suggested the increase of electrical resistivity of C-304L when the oxide film was grown up on the surface of welded 304L.



For corrosion testing of welded 304L and C-304L, the polarization curves obtained from the electrochemical test in NaCl mixed H_2SO_4 solution are shown in Fig. 5 (c). The corrosion rate was measured by Tafel's plot and further calculated by the corrosion penetration rate (CPR) formula [30]. From corrosion rate (Fig. 5 (d)), the welded 304L exhibited high corrosion rate (2.629 mmpy) than those of C-304L specimens with thickness film of 5.5 nm (7.504×10^{-3} mmpy), 30.2 nm (2.148×10^{-3} mmpy) and 40.4 nm (1.091×10^{-3} mmpy), respectively.

4. Conclusion

The stainless steel pipe 304L was welded by the tungsten inert gas (TIG) welding process. The inspection results showed the completed weld of the welded specimen (welded 304L) without any defect and discontinue. By chromic reaction, the surface of welded 304L was successfully oxidation to obtain colored film coated on the surface of the specimen. The XRD pattern of the specimen after oxidation (C-304L) showed mixed phases of austenitic steel and Cr_2O_3 . The crystallite size of chromium oxide was found to be 5 to 30 nm. The results from AFM showed that the increased oxidative time resulted in the increased Cr_2O_3 thickness on the C-304L surface. From surface oxidation, the Cr_2O_3 could improve

the surface properties of welded 304L such as hardness, electrical resistivity, and corrosion resistance. All the results concluded that the C-304L from surface oxidation showed excellent surface resistance for applications related to erosion-corrosion.

5. Acknowledgment

This research was funded by KMUTNB (RES-CIT 0524/2021)

6. References

- [1] ASTM A312/A312M-18, Standard Specification for Seamless, Welded, and Heavily Cold Worked Austenitic Stainless Steel Pipes, 2015.
- [2] M. Naeem, J. Iqbal, M. Zakauallah, M. Shafiq, Z.I. Mujahid, J.C. Díaz-Guillén, C.M. Lopez-Badillo, R.R.M. Sousa, and M.A. Khan, Enhanced wear and corrosion resistance of AISI-304 steel by duplex cathodic cage plasma treatment, *Surface and Coatings Technology*, 2019, 375, 34–45.
- [3] Y. L. He, and Z. B. Xing, Investigations on the microstructure, mechanical properties and corrosion resistance of SUS 304 austenitic stainless steel welded joints by pulsed current gas tungsten arc welding, *Materials Research Express*, 2019, 6, 088001, 1–15.



- [4] X. Wang, Z. Yang, Z. Wang, Q. Shi, B. Xu, C. Zhou, and L. Zhang, The influence of copper on the stress corrosion cracking of 304 stainless steel, *Applied Surface Science*, 2019, 478, 492–498.
- [5] K.S. Prasad, C.S. Rao, and D.N. Rao, A review on welding of AISI 304L austenitic stainless steel, *Journal for Manufacturing Science and Production*, 2014, 14(1), 1–11.
- [6] G.R. Mirshekari, E. Tavakoli, M. Atapour, and B. Sadeghian, Microstructure and corrosion behavior of multipass gas tungsten arc welded 304L stainless steel, *Materials and Design*, 2014, 55, 905–911.
- [7] P.K. Giridharan, and N. Murugan, Optimization of pulsed GTA welding process parameters for the welding of AISI 304L stainless steel sheets, *The International Journal of Advanced Manufacturing Technology*, 2009, 40, 478–489.
- [8] S. Kumar, and A.S. Shahi, Effect of heat input on the microstructure and mechanical properties of gas tungsten arc welded AISI 304 stainless steel joints, *Materials and Design*, 2011, 32, 3617–23.
- [9] X.K. Zhu, and Y.J. Chao, Numerical simulation of transient temperature and residual stresses in friction stir welding of 304L stainless steel, *Journal of Materials Processing Technology*, 2004, 146, 263–272.
- [10] W.S. Lee, C.F. Lin, C.Y. Liu and C.W. Cheng, The effects of strain rate and welding current mode on the dynamic impact behavior of plasma-arc-welded 304L stainless steel weldments, *Metallurgical and Materials Transactions A*, 2004, 35A, 1501–1515.
- [11] T.G. Gooch, Corrosion behavior of welded stainless steel, *Welding Journal*, 1996, 135s–154s.
- [12] A. Wahid, D.L. Olson, and D.K. Matlock, Corrosion of weldments, *ASM Handbook: Welding, Brazing, and Soldering*, 1993, 6, 1065–1069.
- [13] V. Gopalakrishnan, V. BaluSamy, and S.O. Mohammed Rafi, Corrosion study on weldments of austenitic stainless steel, *International Journal of Scientific Research Engineering and Technology*, 2014, 3(5), 897–901.
- [14] M. Aparicio, A. Jitianu, G. Rodriguez, K. Al-Marzoki, M. Jitianu, J. Mosa, and L.C. Klein, Thickness-properties synergy in organic–inorganic consolidated melting-gel coatings for protection of 304 stainless steel in NaCl solutions, *Surface and Coatings Technology*, 2017, 315, 426–435.



- [15] R.T. Loto, C.A. Loto, A.P.I. Popoola, and M. Ranyaoa, Corrosion resistance of austenitic stainless steel in sulphuric acid, *International Journal of Physical Sciences*, 2012, 7(10), 1677–1688.
- [16] E. Kikuti, R. Conrado, N. Bocchi, S.R. Biaggio, and R.C. Rocha-Filho, Chemical and electrochemical coloration of stainless steel and pitting corrosion resistance studies, *Journal of the Brazilian Chemical Society*, 2004, 15, 4, 472–480.
- [17] Z. Cheng, Y. Xue, Z. Tang, L. An and Y. Tian, A one-step process for chemical coloring on stainless steel, *Surface and Coatings Technology*, 2008, 202, 4102–4106.
- [18] C. Tippayasam, J. Palomas, P. Wiman and A. Kaewvilai, Welded stainless steel: Surface oxidation, characterization, hardness and corrosion resistance, *Key Engineering Materials*, 2020, 856, 106-111.
- [19] Z.B. Zheng, and Y.G. Zheng, Effects of surface treatments on the corrosion and erosion-corrosion of 304 stainless steel in 3.5% NaCl solution, *Corrosion Science*, 2016, 112, 657–668.
- [20] J.E. Qu, C. Yu, R. Cui, J. Qin, H. Wang, and Z. Cao, Preparation of super-hydrophobic and corrosion resistant colored films on chemically etched 304 stainless steel substrate, *Surface and Coatings Technology*, 2018, 354, 236–245.
- [21] L.V. Taveira, G. Frank, H.P. Strunk, and L.F.P. Dick, The influence of surface treatments in hot acid solutions on the corrosion resistance and oxide structure of stainless steels, *Corrosion Science*, 2005, 47, 757–769.
- [22] E. Kikuti, N. Bocchi, J.L. Pastol, M.G. Ferreira, M.F. Montemor, M.D.C. Belo, and A.M. Simoes, Composition and structure of coloured oxide films on stainless steel formed by triangular current scan and cathodic hardening treatment, *Corrosion Science*, 2007, 49 2303–2314.
- [23] ASTM D1193-06, Standard Specification for Reagent Water, 2011.
- [24] M.M. Abdullah, F.M. Rajab, and S.M. Al-Abbas, Structural and optical characterization of Cr₂O₃ nanostructures: Evaluation of its dielectric properties, *AIP Advances*, 2014, 4, 027121,1–11.



- [25] N. Srisuwan, N. Kumsri, T. Yingsamphancharoen, and A. Kaewvilai, Hardfacing welded ASTM A572-based, high-strength, low-alloy steel: welding, characterization, and surface properties related to the wear resistance, *Metals*, 2019, 9(2), 244.
- [26] C. Tippayasam, and A. Kaewvilai, Steel reinforced polyethylene corrugated pipe: Extrusion welding, investigation and mechanical testing, *Welding Journal*, 2020, 99(2), 52s-58s.
- [27] ASTM G5-14, Standard Reference Test Method for Making Potentiodynamic Anodic Polarization Measurements, 2014.
- [28] ASME Section V, Nondestructive Examination, 2017.
- [29] S.E. Ziemniak, L.M. Anovitz, R.A. Castelli, and W.D. Porter, Thermodynamics of Cr_2O_3 , FeCr_2O_4 , ZnCr_2O_4 , and CoCr_2O_4 , *The Journal of Chemical Thermodynamics*, 2007, 39(11), 1474–1492.
- [30] T. Yingsamphancharoen, N. Srisuwan, and A. Rodchanarowan, The electrochemical investigation of the corrosion rates of welded pipe ASTM A106 grade B, *Metals*, 2016, 6, 207.